# University of Groningen

## Roughness-dependent wetting behavior of vapor-deposited metallic thin films

Foadi, Farnaz; Allaei, S. Mehdi Vaez; Palasantzas, George; Mohammadizadeh, Mohammad Reza

[Link to publication in University of Groningen/UMCG research database](#)

# Roughness-dependent wetting behavior of vapor-deposited metallic thin films

Farnaz Foadi,[1] S. Mehdi Vaez Allaei,[2] George Palasantzas,[3] and Mohammad Reza Mohammadizadeh[1,*]

[1]*Supermaterials Research Laboratory (SRL), Department of Physics, University of Tehran,*
*North Kargar Avenue, P.O. Box 14395-547, Tehran, Iran*
[2]*Department of Physics, University of Tehran, North Kargar Avenue, P.O. Box 14395-547, Tehran, Iran*
[3]*Zernike Institute for Advanced Materials, University of Groningen, Nijenborgh 4, 9747 AG Groningen, The Netherlands*

We studied the wetting behavior of silver and copper thin films versus their kinetic roughening upon deposition at room temperature on glass substrates. Time-dependent height-height correlation functions were extracted from atomic force microscopy images, and they demonstrated a nonstationary growth front of the film roughness associated with a temporal evolution of the local surface slope. As a result, we tried to correlate the roughness statistical properties such as the root-mean-square (rms) roughness $\sigma$, the correlation length $\xi$, and the local surface slope ($\rho \approx \sigma/\xi$) with the wetting behavior of the films' surfaces. The contact angle behavior was also studied by analyzing the variation of the energy of the system with water penetrating into the surface cavities, and the associated Laplace pressure induced by the local surface curvature. Hence, it was demonstrated that the wetting transition from a metastable Cassie-Baxter state to a Wenzel state as well as the penetration of a droplet into the surface crevices occur at the smaller local surface slopes for the higher surface energy material.

## I. INTRODUCTION

In the last few decades, the subject of wetting has attracted much attention due to its critical importance in diverse applications [1–3]. A major objective in this field is the measurement of the contact angle (CA) at which the liquid-vapor interface meets a solid surface. A surface with CA<90° is considered hydrophilic, while one with CA>90° is termed a hydrophobic surface. Wetting on smooth and rough surfaces could be described in principle by the Young [4] and Cassie-Baxter [5] or Wenzel [6] models, respectively. The Wenzel model concludes that the roughness increment makes a hydrophilic surface more hydrophilic, and a hydrophobic surface more hydrophobic. In the Cassie-Baxter regime, regardless of the nature of a surface, an increasing surface roughness always increases the CA. In any case, the wettability of a solid surface is determined by both the surface chemistry and the morphology [7–9]. For hydrophobic surfaces, there are two possibilities, namely the lotus and the rose petal effects for which the adhesion force is different. Water repellent superhydrophobic surfaces mimicking the lotus leaf have attracted intense investigations due to the self-cleaning applications [10–12]. On the other hand, some surfaces follow the rose petal effect, where a droplet is pinned on the surface prohibiting an easy roll-off [13,14]. Finally, other investigations have been devoted to making hydrophilic coatings from metals and metal oxides [15–18], and a relation between hydrophilicity and some properties such as the photocatalysis has also been observed [19–22].

A theoretical analysis [23] has shown that the CA of a surface depends on the roughness parameters such as the root-mean-square (rms) roughness, the correlation length, and the local roughness exponent. Although the calculations were performed in the weak roughness limit, the CA dependency on the above-mentioned parameters has been well established. Yang *et al.* [24] have investigated the relation between the wettability of a rough surface in contact with hydrocarbon droplets through molecular dynamics calculations. Their findings inspired experimental investigations to show the wetting dependency on the roughness and the fractal parameters. Their results have shown the role of the surface roughness on the CA, whereas the CA was found to be independent of the fractal dimension. The effect of the fractal parameters of ZnO thin films on the wetting was studied by Sarkar *et al.* [25]. They concluded that tuning the wettability of a surface can be performed by altering the morphological parameters. In another work [26], it was shown that higher fractal dimensions lead to higher CAs. Another experimental and theoretical work by Singh *et al.* [27] for nanostructured films, where ion treatment resulted in surfaces with different fractal dimensions, showed higher CAs for surfaces with smaller fractal dimensions. However, there was not a meaningful variation between the CA and the fractal dimension, while the wetting behavior of the films was attributed to the surface chemistry variations due to different ion dosing. Furthermore, in hierarchical surfaces the hydrophobicity can be enhanced due to the existence of multiple structures at the submicron length scale [28,29]. A rather complete study was performed by Yadav *et al.* [30] to explore the role of the roughness exponent and the fractal dimension on the wettability of a rippled surface, where it was found that a higher CA corresponds to a surface with a larger fractal dimension. Jain and Pitchumani [31] tried to generate a fractal model for the wetting of the multiscale random rough surfaces. Their model predicts the CA on hydrophobic and superhydrophilic surfaces, in a good

*zadeh@ut.ac.ir

TABLE I. Surface statistical parameters including the rms roughness amplitude $\sigma$, the correlation length $\xi$, and the roughness exponent $\alpha$ for the different (a) Ag and (b) Cu surfaces. In addition, the thicknesses of all the films deposited at the various deposition times are also included.

| Sample ID | Deposition time (min) | Thickness $\pm10$ (nm) | rms roughness $\sigma$ (nm) | Roughness exponent $\alpha$ | Correlation length $\xi$ (nm) |
|---|---|---|---|---|---|
| | | | (a) Ag surfaces | | |
| S1 | 5 | | $1.20 \pm 0.04$ | $0.89 \pm 0.02$ | $19.0 \pm 0.1$ |
| S2 | 25 | 73 | $2.80 \pm 0.02$ | $0.84 \pm 0.03$ | $24.80 \pm 0.50$ |
| S3 | 50 | 148 | $3.60 \pm 0.30$ | $0.90 \pm 0.05$ | $29.0 \pm 0.2$ |
| S4 | 60 | 184 | $4.50 \pm 0.10$ | $0.88 \pm 0.03$ | $33.0 \pm 0.9$ |
| S5 | 120 | 350 | $5.60 \pm 0.20$ | $0.90 \pm 0.04$ | $40.0 \pm 1.1$ |
| | | | (b) Cu surfaces | | |
| C1 | 10 | | $1.20 \pm 0.02$ | $0.80 \pm 0.07$ | $17.0 \pm 0.3$ |
| C2 | 20 | 63 | $2.30 \pm 0.10$ | $0.86 \pm 0.01$ | $24.0 \pm 1.1$ |
| C3 | 50 | 140 | $2.80 \pm 0.20$ | $0.85 \pm 0.08$ | $29.0 \pm 0.6$ |
| C4 | 60 | 175 | $3.20 \pm 0.30$ | $0.83 \pm 0.01$ | $31.0 \pm 1.3$ |
| C5 | 120 | 348 | $4.0 \pm 0.1$ | $0.88 \pm 0.03$ | $35.0 \pm 1.2$ |

agreement with experiment, which has a strong dependence on the length scales over which the surface asperities are considered but is almost independent of the surface fractal dimension.

So far, however, no experimental work has been performed to compare the wetting behavior of relatively hydrophilic random rough surfaces of different materials and subsequently with different surface energies, with respect to the evolution of their statistical roughness parameters and the associated local surface slopes. For this purpose we deposited silver (Ag) and copper (Cu) thin films at room temperature and compared the wetting behavior versus the evolution of their morphology due to kinetic roughening.

## II. EXPERIMENTAL METHODS

In the present work, Ag and Cu thin films were deposited on soda lime glass (rms roughness $<2.5$ nm) substrates by thermal evaporation (Edwards, ED50 system) under high vacuum (base pressure $\sim 7 \times 10^{-6}$ torr). Before the deposition, the substrates were ultrasonically cleaned in acetone, alcohol, and deionized water to remove any contamination from the surfaces. The metal deposition was performed at the room temperature at a constant power of 3.3 Watt. The distance between the metal target (purity 99.999%) and the substrate was 15 cm, and the deposition rate was kept constant 0.5 Å/s for the both materials. The different samples and their growth conditions are shown in Table I.

The thickness of the films was determined using a stylus profilometer with an accuracy of $\pm10$ nm, where the minimum measurable film thickness was approximately 50 nm. Furthermore, the morphology of the films was measured by an NT-MDT atomic force microscope (AFM) operated in the semicontact mode using $Si_3N_4$ tips. For each sample we obtained seven AFM images with $1024 \times 1024$ pixels at different locations for averaging purposes. All the corresponding morphological parameters were calculated and averaged over seven images of each sample. The structure of the thin films was determined using grazing incidence x-ray diffraction (GIXRD; PANalytical, X'Pert Pro) at an incidence angle of $w = 2°$ operating at 40 kV and 40 mA.

Finally, the wetting properties of the water droplets on the samples were investigated using a CA measuring system. For this purpose, droplets from distilled deionized water with the volume of $\sim 5$ $\mu$l were used on four different locations of each sample, and the CA images were recorded by a coupled CCD camera. The measurements were carried out using ax-isymmetric drop shape analysis plugin in IMAGEJ software, and were averaged for the different droplets on the surface. It should be noted that CA measurements were performed within one week after sample preparation and also at random within three days after the first day of measurements; the samples were kept in sealed containers after measurements to reduce the effect of hydrocarbon adsorption from the ambient atmosphere. In addition, we repeated the CA measurements about one year after deposition to investigate the effect of hydrocarbons on the wetting behavior of thin films versus the corresponding surface morphology.

## III. RESULTS AND DISCUSSION

### A. Surface roughness characterization

Figure 1 depicts $\theta/2\theta$ diffractograms for the thick (a) Ag and (b) Cu films. The peaks were identified by comparing with JCPDS cards No. 03-0931 and No. 43-1038 for Ag and AgO phases corresponding to different planes without any impurity phase. In addition, the x-ray diffraction (XRD) pattern for the Cu sample exhibited a cubic crystalline structure without any impurity according to JCPDS card No. 04-0836. In addition, these patterns show that both the Ag and Cu films have a polycrystalline nature and the (111) peak is stronger than the other peaks in the growth of the thin films.

It is noteworthy that, due to the high vacuum pressure for our system and also exposure to air after the deposition, the oxide phases are present in the XRD diffractograms. However, independently of any oxidation in the bulk of the films during evaporation, the formation of a thin oxide layer of $\sim 1$–3 nm thick will be always inevitable under these film preparation conditions and the surface energy of this metal oxide thin layer will play dominant role on the wetting process rather than the bulk of the film [32].
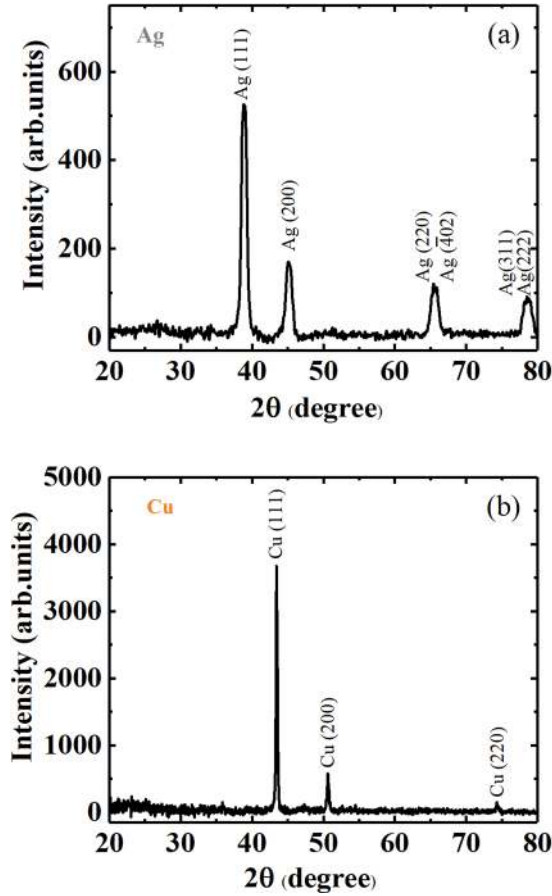
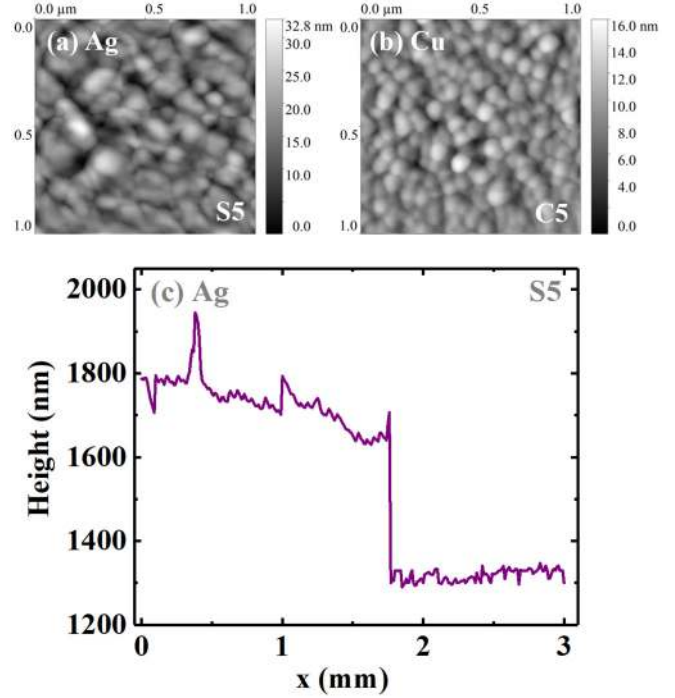FIG. 1. GIXRD spectrum of (a) S5 (Ag) and (b) C5 (Cu) samples.



FIG. 2. 2D AFM images of thick (a) Ag (sample S5) and (b) Cu (sample C5) surfaces. Plot (c) shows the section height profile of sample S5 as an example by a stylus profilometer tracing a distance of 3 mm along a step to determine the film thickness.

Figure 2 shows the AFM images of the thick (a) Ag and (b) Cu surfaces taken over a scan area of $1 \times 1 \, \mu m^2$, where also in plot (c) the step height profile of an Ag surface is indicated to obtain the film thickness (~350 nm in this case). The topography of the film's surfaces changes with increasing film deposition time, forming also larger grains or larger correlation lengths (see also Table I).

The growth front roughening of a surface evolving in time can be described by the time-dependent height-height correlation function $H(\vec{r}, t) = \langle [h(\vec{r}, t) - h(0, t)]^2 \rangle$ [33] (see Fig. 3), where $h(\vec{r}, t)$ is the surface height at the growth time t and $\langle \cdots \rangle$ denotes statistical average over topography data. The correlation function $H(\vec{r}, t)$ shows a scaling behavior at small length scales that is followed by a saturation regime at larger length scales. The upward movement of the function with increasing deposition time at small length scales, $r \ll \xi$ with $\xi$ the lateral correlation length, is a clear sign of an anomalous growth [34]. In this case, the local surface slope is no longer time invariant in the growth process, leading to formation of locally rougher surfaces due to limited surface diffusion. For many surfaces the height-height correlation function scales according to the Family-Vicsek scaling theory [35] represented by the form $H(\vec{r}, t) = 2[\sigma(t)]^2 f(\vec{r}/\xi(t))$, where $f(x)$ is a scaling function. In any case, the measurement of $H(\vec{r}, t) = \langle [h(\vec{r}, t) - h(0, t)]^2 \rangle$ allows determination of all the statistical parameters, namely, the rms roughness amplitude $\sigma$, the roughness exponent $\alpha$, and the lateral correlation

length $\xi$, since it follows the scaling behavior [36,37]

$$H(\vec{r}, t) = \begin{cases} \propto r^{2\alpha}, & r \ll \xi, \\ 2\sigma^2, & r \gg \xi. \end{cases} \quad (1)$$

The roughness exponent $\alpha$ $(0 < \alpha < 1)$, which for smaller values gives more jagged surfaces at the short length scales $(<\xi)$, can be calculated from the linear fit of the log-log plot of the correlation function at $r < \xi$. The correlation length $\xi$ can be determined from the intersection of the linear part with the saturation regime at $r \gg \xi$ that yields the value of the rms roughness amplitude $\sigma$.

From Fig. 3 the measured local roughness exponents for the Ag and Cu were $\alpha = 0.88 \pm 0.03$ and $\alpha = 0.84 \pm 0.03$, respectively; almost the same within the error bars of the measurements. The large value of $\alpha$ indicates that the dominant surface relaxation during growth is surface diffusion [35]. The interface width or rms roughness $(\sigma)$ of all samples was calculated using the AFM data, where especially for the case of Cu it does not change considerably with the deposition time. The latter can be attributed to the large surface mobility of the Cu atoms even at room temperature deposition [38].

In Fig. 4 we have plotted the local surface slope $\rho \approx \sigma/\xi$, which is a measure of the long wavelength undulations on the surface [39].

It should be noted that for more precise calculations of $\rho$ one can use the analytic form [40]

$$\rho = \frac{\sigma}{\xi \sqrt{2}} \left( \frac{1}{1 - \alpha} ([1 + c(Q_c \xi)^2]^{1-\alpha} - 1) - 2c \right)^{1/2}, \quad (2)$$
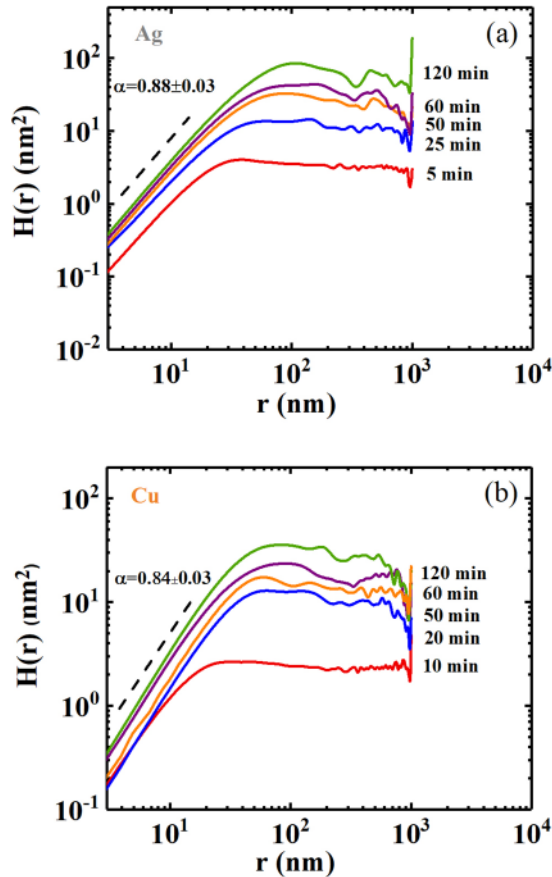
FIG. 3. The time-dependent height-height correlation function for (a) Ag and (b) Cu samples.

where $c = (1/2\alpha)(1 - [1 + c(Q_c\xi)^2]^{-\alpha})$ for $0 < \alpha \leqslant 1$ [39], and $Q_c = \pi/a_o$ with $a_o$ the lowest lateral roughness cutoff, typically of atomic dimensions. For large roughness exponents $\alpha \sim 1$, as is the case here for the evaporated Ag and Cu films, the local slope can be approximated by the simpler expression $\rho \approx \sigma/\xi$. It is clear from this plot that the anomalous growth of the Ag and Cu thin films is due to the temporal evolution of the local surface slope.
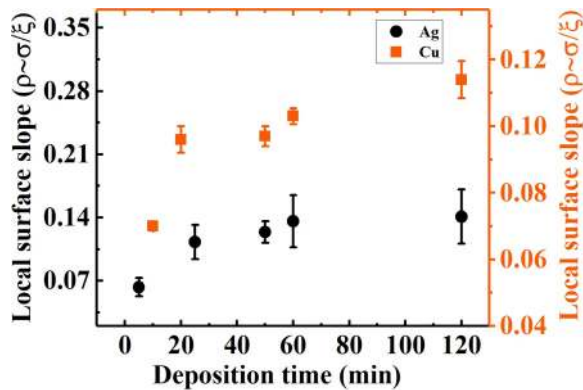


FIG. 4. The local surface slope variation versus the deposition time for the Ag and Cu samples.
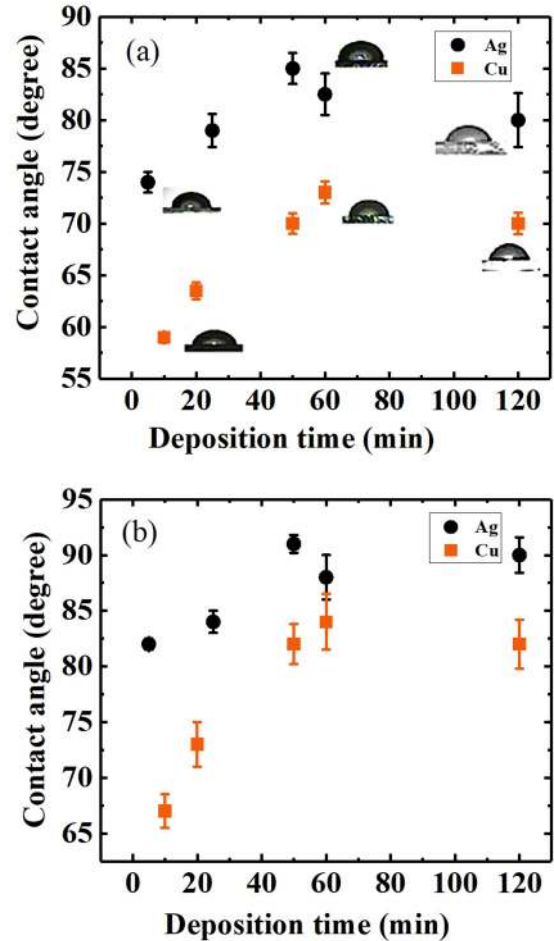


FIG. 5. The variation of the contact angle versus the deposition time (a) for the as-prepared Ag and Cu samples and (b) for the samples after one year.

### B. Contact angle measurements and a theoretical modeling

Figure 5(a) shows an increasing trend in the behavior of the equilibrium static water CA with the deposition time for both Ag and Cu, followed by a decreasing trend. Figure 5(b) shows similar measurements after almost one year to illustrate the effect of adsorbed surface hydrocarbons. We can observe that the almost flat surfaces in Fig. 5(a) for both growing systems (e.g., samples S1 and C1) show the smallest CA. It seems that a droplet wets the crevices on the surface, as can be expected for surfaces with small rms roughness [23,40].

Further, we studied the wetting behavior of the films with respect to the statistical parameters such as the rms roughness $\sigma$ and the correlation length $\xi$ in Figs. 6 and 7. In both cases the CA shows an increasing trend followed by a decreasing trend, as in Fig. 5(a).

Figure 8 also demonstrates the variation of CA with respect to the local surface slope $\rho \approx \sigma/\xi$. The main conclusion from this plot is that the CA on the surface increases with increasing local slope for both Ag and Cu films, and after a point it decreases, which is the same trend as mentioned for the previous plots.

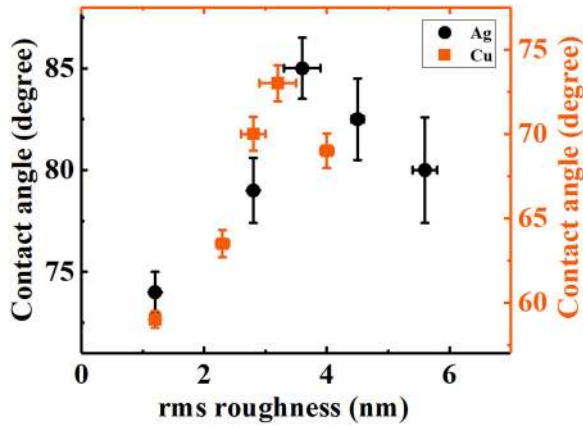From Fig. 8 it appears that there is a competition between the rms roughness $\sigma$ and the correlation length $\xi$ for the

FIG. 6. The contact angle versus the rms roughness for the Ag (solid circle) and Cu (solid square) samples.



FIG. 8. The contact angle versus the local surface slope for the Ag (solid circle) and Cu (solid square) samples. The inset illustrates the relevant roughness parameters and the local surface slope as the water penetrates the surface crevices.

determination of the CA. Although $\sigma$ and $\xi$ increase with the deposition time (see Table I), since the CA first increases and then decreases with respect to both of these parameters, the role of the local slope $\rho$ in determining the CA seems important. For the Cu samples, due to slow temporal evolution of the rms roughness, the variation of the local slope $\rho$ does not change considerably during the deposition ($\rho \sim 0.07$ to $0.11$) and this can be due to the small variation in the surface roughness of the Cu films, as mentioned earlier [Table I(b)]. However, for the Ag and Cu films that are studied in this paper, the small local surface slope value results in the transition from the metastable Cassie-Baxter state to the Wenzel state due to the hydrophilic nature of these metals. This wetting transition was also reported in hydrophilic Cu sputtered films [32]. The mechanism of this transition is rather obscure, but we tried to elucidate this point with the variation of the Laplace pressure and energy of the system per unit cell by penetrating water into the surface pores. Note that the Laplace pressure generated by the weight of a 5 μl water droplet, assuming a spherical shape, will be $P = 2\gamma/r = 136$ Pa since $r = 1.06$ mm and $\gamma = 72$ mN/m [41] for the water-air interfacial tension. In addition, the effect of the gravitation on the shape of the droplet is negligible since the droplet radius
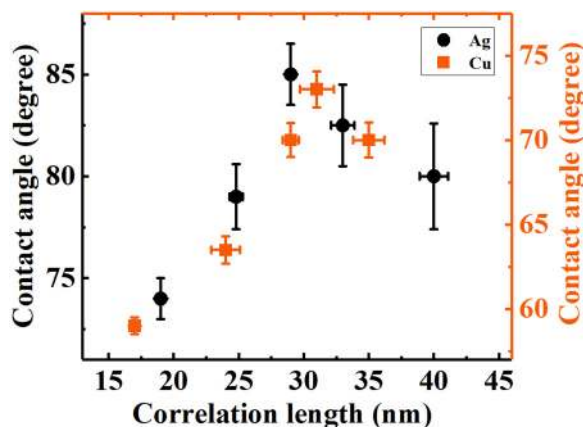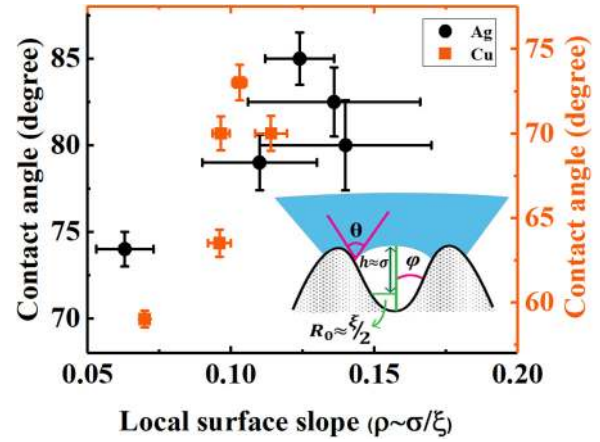
is much smaller than the water capillary length ($l \approx 2.7$ mm) [42].

According to the literature [43], the Laplace pressure for inclined side wall structures is given by

$$\Delta P = P - P_0 = -\frac{\gamma \cos (\theta - \varphi)}{R_0 + h \tan\varphi}, \tag{3}$$

in which $P$ is the pressure in the water, $P_0$ is the air pressure within the surface cavity pore, $\gamma$ is the water-air interfacial tension, $\theta$ is the Young CA on the wall, $\varphi$ is the inclination angle defined as $\varphi \approx \pi/2 - \tan^{-1}(\sigma/\xi)$, $R_0 \approx \xi/2$ is a measure of the surface correlation length, and $h \approx \sigma$ is a measure of the surface height. The inset of Fig. 8 illustrates the relevant roughness parameters and the local surface slope. In addition, if we consider for simplicity that the random roughness resembles conical arrays, then the energy of a system, per unit cell, constituting a checkerboard with the dimension $\xi$ representing the size of the surface peaks, can be written as

$$E = \gamma(\xi^2 - \pi x^2) + (\gamma_{\rm sl} - \gamma_{\rm sv})(\text{cone area})$$
$$= \gamma\xi^2 - \gamma\pi x^2[1 + \cos\theta(1 + \tan Y^2)^{\frac{1}{2}}], \tag{4}$$

with $\tan Y = \sigma/\xi$ denoting the slope of the surface peak. Considering now $\theta = 73°$ and $52°$ for smooth Ag and Cu surfaces [44,45], respectively, we calculated $\Delta P$ and $E$ for both metallic surfaces, and the results are presented in Fig. 9.

From this plot it is clear that for both surfaces $|\Delta P| \ll 1$ (and $\Delta P < 0$), which means that the pressure from the meniscus side of the droplet is smaller than the pressure acting upward from the gas in the cavity beneath the droplet. The latter supports a Cassie-Baxter wetting regime in which the droplet cannot penetrate the surface cavities. On the other hand, the energy of the system per unit cell $E$ is negative, and with increasing deposition time or equivalently increasing roughness it becomes even more negative, favoring the system to be in the Wenzel regime. Therefore, due to the hydrophilic nature of the Ag and Cu surfaces and also the negative energy of the systems, we can conclude that both systems are more
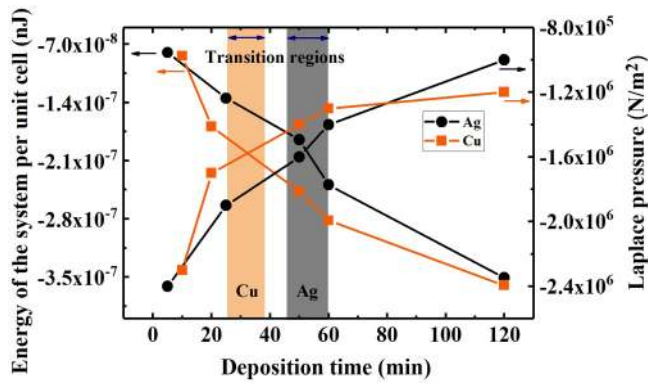


FIG. 7. The contact angle versus the correlation length for the Ag (solid circle) and Cu (solid square) samples.

FIG. 9. The energy of the system per unit cell, *E*, and the Laplace pressure variations of the Ag (solid circle) and Cu (solid square) samples with respect to the deposition time.

likely to be in a Wenzel state. The first part of the CA behavior, where we observe an increasing CA with increasing deposition time, is likely to be a metastable Cassie-Baxter state that finally leads to lower CAs and a Wenzel state. From Fig. 9 it is clear that for Cu, with a higher surface energy compared to Ag, the wetting transition from the metastable Cassie-Baxter state to the Wenzel state occurred at the smaller local surface slopes, showing a higher affinity of the high surface energy material to the water. In addition, it should be noted that the small values of the local surface slopes ($\rho \approx 0.12$ for Ag and $\rho \approx 0.10$ for Cu) result in water penetration into the surface cavities, favoring the wetting transition towards a Wenzel state.

Finally, we repeated the CA measurements one year after synthesizing the samples to explore how hydrocarbon adsorption and aging effects can alter the wetting behavior of the Ag and Cu surfaces. Hydrocarbon adsorption has been addressed in the literature [46,47], showing that this effect should be carefully considered in the wetting phenomena. To reduce the hydrocarbon adsorption from air, we performed the CA measurements of the as-prepared Ag and Cu, while keeping them in evacuated sealed containers before and after the measurements. However, one year after the preparation, CA on each surface has grown to some degree, as a sign

of aging and hydrocarbon adsorption [see Fig. 5(b)]. The interesting point in this later set of experiments is the similar behavior of the CA with the deposition time or rms roughness compared to what we obtained for the as-prepared samples [if we compare with Fig. 5(a)], illustrating the strong role of the surface roughness on the CA behavior besides the chemistry of the surfaces. The results are consistent with Cu sputtered thin films too [32].

## IV. CONCLUSIONS

In this work, we studied the wetting behavior of silver and copper thin films versus their kinetic roughening upon deposition at room temperature on glass substrates. Time-dependent height-height correlation functions were extracted from atomic force microscopy images, and they demonstrated a nonstationary growth front of the film roughness associated with a temporal evolution of the local surface slope. As a result we tried to correlate the roughness statistical properties such as the root-mean-square (rms) roughness $\sigma$, the correlation length $\xi$, and the local surface slope ($\rho \approx \sigma/\xi$) with the wetting behavior of the films' surfaces. The contact angle behavior was also studied by analyzing variation of the energy of the system with water penetrating into the surface cavities, and the associated Laplace pressure induced by the local surface curvature. Hence, it was demonstrated that the wetting transition from a metastable Cassie-Baxter state to a Wenzel state as well as the penetration of a droplet into the surface crevices occurs at smaller local surface slopes for the higher surface energy material. Finally, the effect of the roughness on the contact angles still remains present after prolonged exposures to ambient conditions leading to the enhanced hydrocarbon adsorption and aging of both metallic systems.

[1] R. Fürstner, W. Barthlott, C. Neinhuis, and P. Walzel, Langmuir **21**, 956 (2005).

[2] T. M. Squires and S. R. Quake, Rev. Mod. Phys. **77**, 977 (2005).

[3] N. Gao, Y. Y. Yan, X. Y. Chen, and D. J. Mee, Mater. Lett. **65**, 2902 (2011).

[4] T. Young, Philos. Trans. R. Soc. Lond **95**, 65 (1805).

[5] A. B. D. Cassie and S. Baxter, Trans. Faraday Soc. **40**, 546 (1944).

[6] R. N. Wenzel, Ind. Eng. Chem. **28**, 988 (1936).

[7] D. 't Mannetje, S. Ghosh, R. Lagraauw, S. Otten, A. Pit, C. Berendsen, J. Zeegers, D. van den Ende, and F. Mugele, Nat. Commun. **5**, 3559 (2014).

[8] P. G. de Gennes, Rev. Mod. Phys. **57**, 827 (1985).

[9] A. Tuteja, W. Choi, J. M. Mabry, G. H. McKinley, and R. E. Cohen, Proc. Natl. Acad. Sci. USA **105**, 18200 (2008).

[10] R. Akbari, G. Ramos Chagas, G. Godeau, M. Mohammadizadeh, F. Guittard, and T. Darmanin, Appl. Surf. Sci. **443**, 191 (2018).

[11] K. Koch, B. Bhushan, Y. C. Jung, and W. Barthlott, Soft Matter **5**, 1386 (2009).

[12] S. Nishimoto and B. Bhushan, RSC Adv. **3**, 671 (2012).

[13] L. Feng, Y. Zhang, J. Xi, Y. Zhu, N. Wang, F. Xia, and L. Jiang, Langmuir **24**, 4114 (2008).

[14] J. Long, P. Fan, D. Gong, D. Jiang, H. Zhang, L. Li, and M. Zhong, ACS Appl. Mater. Interfaces **7**, 9858 (2015).

[15] M. Shibuya and M. Miyauchi, Adv. Mater. **21**, 1373 (2009).

[16] A. A. Ashkarran and M. R. Mohammadizadeh, Mater. Res. Bull. **43**, 522 (2008).

[17] G. Valette, J. Electroanal. Chem. Interfacial Electrochem. **139**, 285 (1982).

[18] J. Drelich, E. Chibowski, D. D. Meng, and K. Terpilowski, Soft Matter **7**, 9804 (2011).

[19] M. Kazemi and M. R. Mohammadizadeh, Thin Solid Films **519**, 6432 (2011).

[20] M. Kazemi and M. R. Mohammadizadeh, Appl. Surf. Sci. **257**, 3780 (2011).

[21] S. Kimiagar and M. R. Mohammadizadeh, Eur. Phys. J. - Appl. Phys. **61**, 10303 (2013).

[22] M. Miyauchi, Phys. Chem. Chem. Phys. **10**, 6258 (2008).

[23] G. Palasantzas and J. T. M. de Hosson, Acta Mater. **49**, 3533 (2001).

[24] C. Yang, U. Tartaglino, and B. N. J. Persson, Phys. Rev. Lett. **97**, 116103 (2006).

[25] S. Sarkar, S. Patra, N. Gayathri, and S. Banerjee, Appl. Phys. Lett. **96**, 063112 (2010).

[26] S. Patra, S. Sarkar, S. K. Bera, G. K. Paul, and R. Ghosh, J. Appl. Phys. **108**, 083507 (2010).

[27] U. B. Singh, R. P. Yadav, R. Kumar, S. Ojha, A. K. Mittal, S. Ghosh, and F. Singh, J. Appl. Phys. **122**, 185303 (2017).

[28] F. De Nicola, P. Castrucci, M. Scarselli, F. Nanni, I. Cacciotti, and M. De Crescenzi, Sci. Rep. **5**, 8583 (2015).

[29] P. K. Dhillon, P. S. Brown, C. D. Bain, J. P. S. Badyal, and S. Sarkar, Appl. Surf. Sci. **317**, 1068 (2014).

[30] R. P. Yadav, T. Kumar, V. Baranwal, Vandana, M. Kumar, P. K. Priya, S. N. Pandey, and A. K. Mittal, J. Appl. Phys. **121**, 055301 (2017).

[31] R. Jain and R. Pitchumani, Langmuir **33**, 7181 (2017).

[32] F. Foadi, G. H. ten Brink, M. R. Mohammadizadeh, and G. Palasantzas, J. Appl. Phys. **125**, 244307 (2019).

[33] J. T. Drotar, Y.-P. Zhao, T.-M. Lu, and G.-C. Wang, Phys. Rev. E **59**, 177 (1999).

[34] Y.-P. Zhao, G.-C. Wang, and T.-M. Lu, *Characterization of Amorphous and Crystalline Rough Surface: Principles and Applications* (Academic, New York, 2001).

[35] A.-L. Barabási and H. E. Stanley, *Fractal Concepts in Surface Growth* (Cambridge University Press, Cambridge, 1995).

[36] G. Palasantzas and J. Krim, Phys. Rev. B **48**, 2873 (1993).

[37] G. Palasantzas and J. Krim, Phys. Rev. Lett. **73**, 3564 (1994).

[38] H. P. Bonzel, in *Surface Physics of Materials*, edited by J. M. Blakely (Academic, New York, 1975).

[39] J. Krim and G. Palasantzas, Int. J. Mod. Phys. B **9**, 599 (1995).

[40] G. Palasantzas and G. Palasantzas, Phys. Rev. B **48**, 14472 (1993); **49**, 5785 (1994); G. Palasantzas, Phys. Rev. E **56**, 1254 (1997).

[41] N. R. Pallas and Y. Harrison, Colloids Surf. **43**, 169 (1990).

[42] P.-G. de Gennes, F. Brochard-Wyart, and D. Quéré, in *Capillarity Wetting Phenom. Drops Bubbles Pearls Waves*, edited by P.-G. de Gennes, F. Brochard-Wyart, and D. Quéré (Springer, New York, 2004), pp. 33–67.

[43] Y. Tsori, Langmuir **22**, 8860 (2006).

[44] Y. Zhou, M. Li, B. Su, and Q. Lu, J. Mater. Chem. **19**, 3301 (2009).

[45] M. Yekta-fard and A. B. Ponter, J. Adhes. **18**, 197 (1985).

[46] M. K. Bernett and W. A. Zisman, J. Phys. Chem. **74**, 2309 (1970).

[47] L. B. Boinovich, A. M. Emelyanenko, A. S. Pashinin, C. H. Lee, J. Drelich, and Y. K. Yap, Langmuir **28**, 1206 (2012).